Neutron matter based on consistently evolved chiral three-nucleon interactions

K. Hebeler and R. J. Furnstahl

Neutron matter based on consistently evolved chiral three-nucleon interactions

K. Hebeler[1, *] and R. J. Furnstahl[1, †]

[1]*Department of Physics, The Ohio State University, Columbus, OH 43210, USA*

We present the first results for the neutron matter equation of state (EOS) using nucleon-nucleon and three-nucleon chiral effective field theory interactions that are consistently evolved in the framework of the Similarity Renormalization Group (SRG). The dependence of the EOS on the SRG resolution scale is greatly reduced when induced three-nucleon forces (3NF) are included and the residual variation, which in part is from missing induced four-body interactions, is comparable to estimated many-body perturbation theory truncation errors. The relative growth with decreasing resolution of the 3NF contributions to the energy per neutron is of natural size, but it accelerates at the lowest resolutions where strong renormalization of the long-range 3NF matrix elements is also observed.

Chiral effective field theory (EFT) [1] offers a systematic expansion of nuclear forces well suited to meet the calculational challenges of neutron matter, which span the extremes of low-density universal properties to the dense matter in neutron stars. Conversely, neutron matter provides a powerful laboratory for testing chiral EFT power counting at relevant nuclear densities, since only long-range three-nucleon forces (3NF) contribute at next-to-next-to-leading order (N^{2}LO) [2] and there are no new parameters for three-nucleon (3N) and four-nucleon interactions at next-to-next-to-next-to-leading order (N^{3}LO) [1]. For example, it was recently shown that 3NF at N^{3}LO give relatively large contributions to the neutron matter equation of state (EOS) [3, 4], which may indicate that a chiral EFT with explicit delta degrees of freedom would be more efficient.

At present, the largest uncertainties in microscopic calculations of neutron matter based on chiral EFT interactions are because the low energy constants in the Hamiltonian are not all well determined. This leads to uncertainties in observables such as the nuclear symmetry energy and radii of neutron stars [5]. However, direct calculations based on chiral interactions using many-body perturbation theory (MBPT) also have non-negligible theoretical uncertainties due to truncations of the many-body expansion [3, 4]. Renormalization group (RG) evolution of nuclear interactions to lower resolution scales significantly improves the convergence of MBPT, but in prior calculations three-nucleon interactions have not been evolved consistently [2]. Here we present the first results for the neutron matter equation of state based on consistently evolved chiral nucleon-nucleon (NN) and 3N forces (see Fig. 1). These results show how RG transformations can enable simplified and efficient many-body calculations for neutron matter with controlled theoretical error bars.

We build upon Ref. [6], which presented a framework for the simultaneous evolution of nuclear NN and 3N interactions in a continuous plane-wave (momentum) basis via the Similarity Renormalization Group (SRG). This is

an alternative to using a harmonic oscillator basis [7]. It provides independent checks of the SRG evolution, easier access to alternative SRG generators (see Refs. [8, 9]) and a means to test approximations for induced 3NF [6]. The momentum-space matrix elements can be easily transformed to an oscillator basis for use in calculations of finite nuclei by configuration interaction [10], coupled cluster [11, 12], in-medium SRG methods [13, 14], self-consistent Gorkov Green's function theory [15] or for nuclear shell-model calculations [16].

Most important in the present context is that these
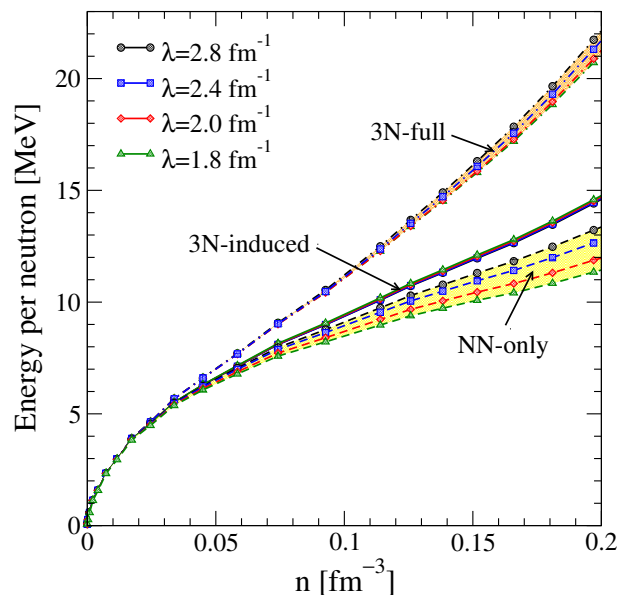
FIG. 1. (Color online) Energy per neutron as a function of neutron density for different SRG resolution scales. The results are grouped according to whether no induced 3NF are included (NN-only), the induced 3NF are included but no initial 3NF (3N-induced), or initial and induced 3NF are included (3N-full). The initial interaction is the 500 MeV N^{3}LO NN potential from Ref. [17] combined with the N^{2}LO 3NF using the consistent low-energy constants $c_1 = -0.81\,\mathrm{GeV}^{-1}$ and $c_3 = -3.2\,\mathrm{GeV}^{-1}$ [2].
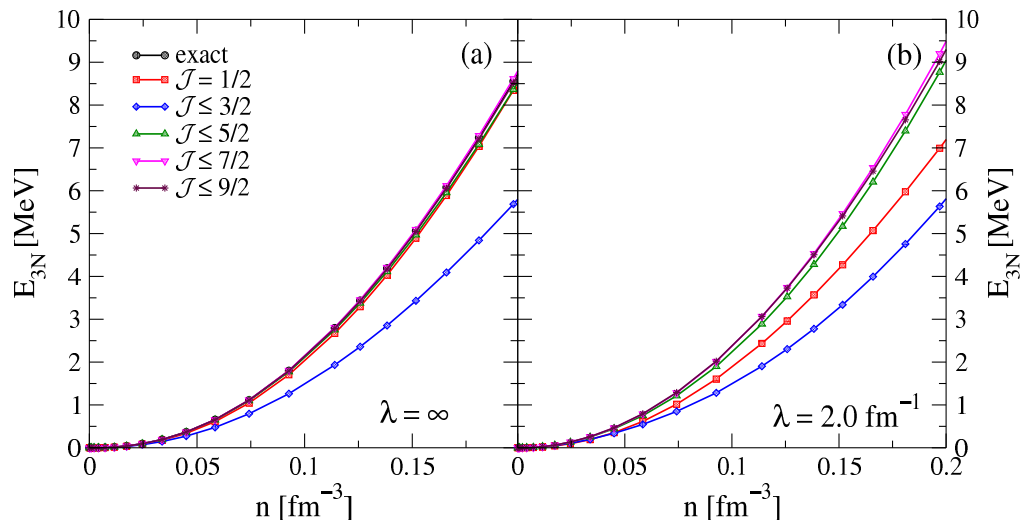
FIG. 2. (Color online) Partial-wave convergence of the Hartree-Fock 3NF-only energy per neutron as a function of density at two different resolution scales. Panel (a) shows the results before evolution ($\lambda = \infty$) and panel (b) at $\lambda = 2.0\,\mathrm{fm}^{-1}$. The Hamiltonian is the same as for the 3N-full results in Fig. 1. For $\lambda = \infty$, only $\mathcal{J} \leq 5/2$ give significant contributions so the lines for the higher partial waves are nearly indistinguishable from the exact result.

evolved interactions can be directly applied in microscopic calculations of the nuclear EOS. Applications to the triton in Ref. [6] verified that nuclear interactions at low resolution scales contain much weaker couplings between low and high-momentum states. This renders the nuclear many-body problem more perturbative and therefore more tractable, with all low-energy observables preserved exactly when all induced contributions are included. However, recent results for finite nuclei using oscillator-evolved 3NF found that high-momentum parts of the chiral two-pion-exchange 3NF led to significant resolution-scale dependence and overbinding in medium-mass nuclei [18, 19]. Neutron matter provides a test laboratory (although limited, because only neutrons) to study if these systematics carry over to infinite matter in MBPT with the new evolution scheme. We have direct access to the form of the 3NF and the scaling behavior of their contributions to the energy as a function of the resolution scale.

The SRG flow equations we solve can be written in the form [20]

$$\frac{dH_s}{ds} = [\eta_s, H_s] \; , \qquad (1)$$

where $H_s = T_{\rm rel} + V_s$ denotes the Hamiltonian as a function of the flow scale parameter s, and η_s labels the generator of the RG transformations. In practice it is more informative to replace s with the resolution (or decoupling) scale $\lambda = s^{-1/4}$, which has units of momentum. Here we choose $\eta_s = [T_{\rm rel}, H_s]$ with the relative kinetic energy $T_{\rm rel}$, as in Ref. [6] and most prior investigations. With this η_s the flow equation generates a continuous series of unitary transformations that renormalizes the Hamiltonian (and all other operators), driving H_s towards a diagonal form

in momentum space [21]. We recast Eq. (1) into separate flow equations for the matrix elements of the NN and 3N interactions [6, 20] and solve them simultaneously in a momentum partial-wave basis.

For the NN forces we use a standard partial-wave basis of the form $|p; (LS)JT\rangle$, where p is the relative momentum and L, S, J and T are the orbital angular momentum, spin, total angular momentum and isospin of the interacting pair. For the three-body basis we choose

$$|p_i q_i; [(LS)J(ls_i)j] \, \mathcal{J}\mathcal{J}_z (Tt_i)\mathcal{T}\mathcal{T}_z\rangle \equiv |pq\alpha\rangle_i \; , \quad (2)$$

where p_i and q_i are the three-body Jacobi momenta of particle i. The quantum numbers l, $s_i = 1/2$, j and $t_i = 1/2$ are the orbital angular momentum, spin, total angular momentum and isospin of particle i relative to the center-of-mass of the pair with momentum p. $\mathcal{J}$ and $\mathcal{T}$ are the total three-body angular momentum and isospin quantum numbers (for details see Refs. [22, 23]). The 3NF at chiral order N^{2}LO are independent of the projections $\mathcal{J}_z$ and $\mathcal{T}_z$ [1]. We use α to abbreviate the angular momentum and isospin quantum numbers.

In the SRG evolution we take all NN interaction matrix elements up through $J_{\max} = 7$ into account, and for the 3NF matrix elements we include all interactions up through $\mathcal{J} = 9/2$ and $J_{\max} = l_{\max} = 5$. In Fig. 2 we show the convergence of the partial-wave 3NF contributions in the Hartree-Fock approximation as a function of density for the initial interaction and after evolution to $\lambda = 2.0\,\mathrm{fm}^{-1}$. While the convergence pattern is somewhat altered after evolution, the partial-wave truncation is reliable at both scales and the results are well converged. The exact Hartree-Fock energy can be calculated without a partial wave expansion for the unevolved in-

teraction [2, 24, 25], and in this case the energy through $\mathcal{J} = 9/2$ is converged within 0.4 percent at nuclear saturation density.

The RG evolution of the 3NF can be performed independently for different values of $\mathcal{J}, \mathcal{T}$ and three-body parity $\pi_3 = (-1)^{L+l}$. For applications to neutron matter we only need matrix elements for the isospin channel $\mathcal{T} = 3/2$. Our calculations are based on antisymmetrized matrix elements of the form

$$\langle pq\alpha|\overline{V}_{123}|p'q'\alpha'\rangle \equiv {}_i\langle pq\alpha|\mathcal{A}_{123}V_{123}^{(i)}\mathcal{A}_{123}|p'q'\alpha'\rangle_i \ , \quad (3)$$

where $V_{123}^{(i)}$ is the i-th Faddeev component of the three-body interaction, $\mathcal{A}_{123} = (1 + P_{123} + P_{132})$ is an antisymmetrizer, and $P_{123}(P_{132})$ is the cyclic (anti-cyclic) permutation operator (see Ref. [22]). Such antisymmetrized matrix elements with two antisymmetrizers, in contrast to partially antisymmetrized matrix elements typically used in Faddeev calculations (see, e.g., Ref [26]), are particularly suitable for solving the SRG flow equations for 3NF (see Ref. [6]). The initial matrix elements are generated directly in this form using a novel automatized partial-wave decomposition for the 3NF [26, 27]. This new method ensures that the interaction is antisymmetrized exactly in spin and isospin space.

Due to the softening of NN and 3N forces during the RG evolution, it is possible to apply MBPT for the calculation of the neutron matter equation of state at low resolution scales. In the present calculations we resum contributions from NN forces in the ladder approximation by averaging the Pauli operator over all angles (for details see Ref. [28]) and using Hartree-Fock single-particle energies. Contributions from 3NF are calculated in Hartree-Fock approximation. Based on results of Ref. [2] we expect this approximation to provide the dominant 3NF contributions at low-resolution scales. We also compute the NN second-order contributions for comparison, which allows us to probe the perturbativeness of the NN interactions as a function of the RG scale λ. The inclusion of higher-order diagrams involving 3NF requires significant computational storage because of the coupling of partial waves with different $\mathcal{J}$ and π. Such calculations are currently in progress.

In the Hartree-Fock approximation, the 3NF contributions to the energy per volume is given by:

$$\frac{E_{HF}}{V} = \frac{1}{18}\prod_{i=1}^{3}\mathrm{Tr}_{\sigma_i}\int\frac{d\mathbf{k}_i}{(2\pi)^3}$$
$$\times \langle 123|\mathcal{A}_{123}V_{123}\mathcal{A}_{123}|123\rangle\, n_{\mathbf{k}_1}n_{\mathbf{k}_2}n_{\mathbf{k}_3} \ , \quad (4)$$

where $n_{\mathbf{k}}$ are the zero-temperature occupation numbers. Compared to the relations of Refs. [2, 28] an extra factor $1/3$ appears because the 3NF are antisymmetrized in the initial and final states. The spin sum in the Jacobi

momentum basis can be expressed in the form

$$\sum_{S,\mu,\nu}\langle\mathbf{pq}S\mu\frac{1}{2}\nu|\mathcal{A}_{123}V_{123}\mathcal{A}_{123}|\mathbf{pq}S\mu\frac{1}{2}\nu\rangle$$

$$= \frac{1}{(4\pi)^2}\sum_{\alpha,\alpha'}\delta_{SS'}\sum_{\bar{L},\mathcal{S},\mathcal{L},\mathcal{J}}\hat{\mathcal{S}}\hat{\mathcal{L}}\hat{\mathcal{J}}\sqrt{\hat{J}\hat{j}\hat{J}'\hat{j}'\hat{L}\hat{L}'\hat{l}\hat{l}'}$$

$$\times (-1)^{l+l'+\mathcal{L}}\mathcal{C}_{l0l'0}^{\bar{L}0}\mathcal{C}_{L0L'0}^{\bar{L}0}P_{\bar{L}}(\hat{\mathbf{p}}\cdot\hat{\mathbf{q}})\,\langle pq\alpha|\overline{V}_{123}|pq\alpha'\rangle$$

$$\times \begin{Bmatrix} L & L' & \bar{L} \\ l' & l & \mathcal{L} \end{Bmatrix}\begin{Bmatrix} L & S & J \\ l & 1/2 & j \\ \mathcal{L} & \mathcal{S} & \mathcal{J} \end{Bmatrix}\begin{Bmatrix} L' & S & J' \\ l' & 1/2 & j' \\ \mathcal{L} & \mathcal{S} & \mathcal{J} \end{Bmatrix} ,\quad (5)$$

using standard notation for the angular momentum coupling, the Clebsch-Gordan coefficients $\mathcal{C}_{l_1m_1l_2m_2}^{l_3m_3}$, and $\hat{x} \equiv \sqrt{2x+1}$.

In Fig. 1 we show the results for the energy per neutron at four different resolution scales λ as a function of neutron number density n. This range of resolution scales has also been used in previous studies of neutron matter and nuclear matter [2, 29] based on $V_{\mathrm{low}\,k}$-evolved NN interactions. The present calculations use the N³LO NN potential ($\Lambda = 500$ MeV) of Ref. [17] plus the consistent 3NF at N²LO with the couplings $c_1 = -0.81\,\mathrm{GeV}^{-1}$ and $c_3 = -3.2\,\mathrm{GeV}^{-1}$ at the initial resolution scale $\lambda = \infty$ ($s = 0$). The other components of the full N²LO 3NF give no contributions in neutron matter [2]. We calculate the EOS in three ways: NN-only, 3N-induced and 3N-full (see Ref. [7] and the caption to Fig. 1). The NN contributions are resummed and the 3NF contributions are calculated in Hartree-Fock approximation. When induced 3NF are taken into account, we find a dramatically reduced λ dependence over the entire density range compared to including only NN forces. When initial 3NF are also included the spread of the results increases, but remains still significantly smaller than the spread of the NN-only results. The 3N-full energy per neutron for $\lambda = 2.0\,\mathrm{fm}^{-1}$ at saturation density is about 0.5–1.5 MeV higher than found in calculations with the same initial NN interaction but with the unevolved N²LO 3NF included with a cutoff ranging from 2.0–2.5 fm^{-1} [2]. More detailed comparisons will be made in a future publication.

In Fig. 3 we show the energy per neutron at nuclear saturation density for two different NN interactions as a function of the resolution scale. Panel (a) uses the NN and 3N interactions as in Fig. 1 and panel (b) uses the N²LO potential ($\Lambda/\tilde{\Lambda} = 450/500$ MeV) of Ref. [30] plus the consistent 3NF with the low-energy constants $c_1 = -0.81\,\mathrm{GeV}^{-1}$ and $c_3 = -3.4\,\mathrm{GeV}^{-1}$. The bands in both panels at the right side indicate the size of unevolved second-order contributions containing NN and 3N forces; these diagrams can be evaluated at the initial RG scale using the framework of Ref. [2]. The band is smaller in panel (b) due to the smaller initial cutoff of the NN potential.

The variation of the energy in the 3N-full case is always within the width of the band. This suggests that the in-
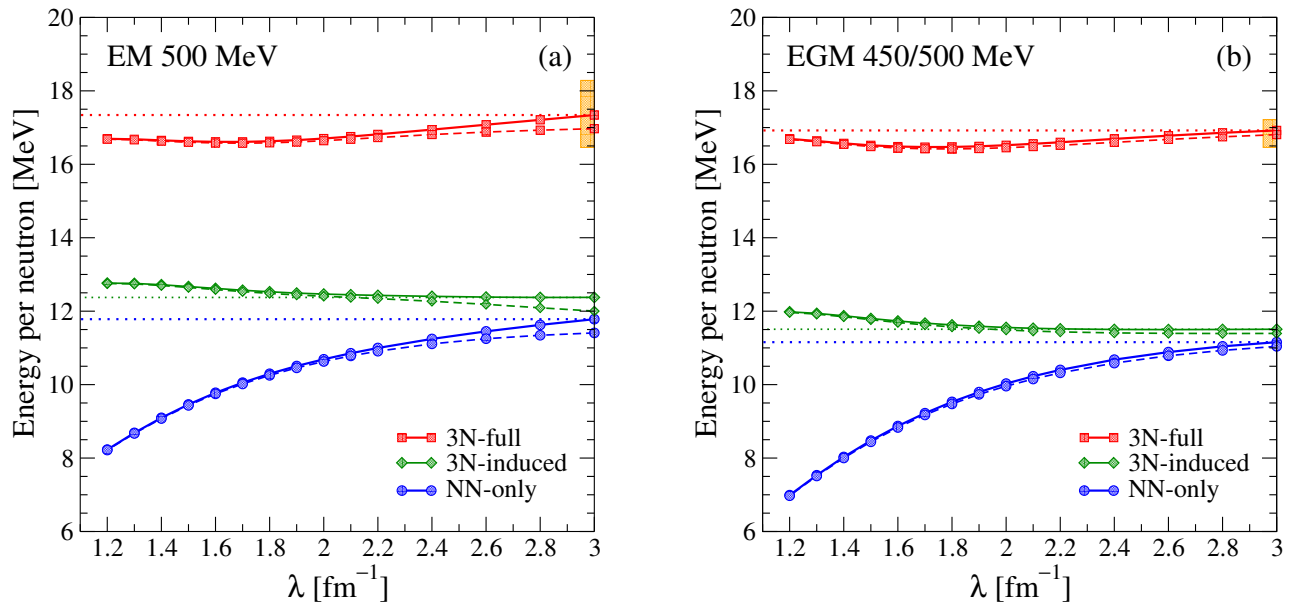
FIG. 3. (Color online) Energy per neutron as a function of the resolution scale λ at nuclear matter saturation density $n_s = 0.16\,\mathrm{fm}^{-3}$ for two different interactions. Panel (a) uses the NN and 3N potentials as in Fig. 1 and panel (b) uses the N^{2}LO potential ($\Lambda/\tilde{\Lambda} = 450/500$ MeV) of Ref. [30] plus the consistent 3NF with the low-energy constants $c_1 = -0.81\,\mathrm{GeV}^{-1}$ and $c_3 = -3.4\,\mathrm{GeV}^{-1}$. The same three calculations (NN-only, 3N-induced, and 3N-full) from Fig. 1 are used here. The solid lines are energies using a resummed particle ladder sum of the NN contributions, with the straight dotted lines marking the energies at $\lambda = 3.0\,\mathrm{fm}^{-1}$. The dashed lines are energies including up to second-order for the NN contributions. The shaded areas at the right indicate the magnitude of the attractive second-order contribution from unevolved NN and 3N forces.

clusion of neglected second-order diagrams with 3NF at finite λ, which are attractive and should decrease in magnitude with decreasing λ [2], may systematically reduce the observed variation with λ above $2.0\,\mathrm{fm}^{-1}$. The small increase in energy below $\lambda = 2.0\,\mathrm{fm}^{-1}$ for both 3N-full and 3N-induced curves might be attributed to induced four-body forces. However, although the size of the variation is of comparable size to contributions from chiral 4N forces in delta-less EFT (see Refs. [3, 31]), it would be premature to draw quantitative conclusions.

The inclusion of induced 3NF contributions greatly reduces the resolution-scale dependence of the EOS even at the present truncation of the many-body expansion. In the left/right panel of Fig. 3 we find a maximal energy variation of about 390/470 keV for the 3N-induced calculations and 650/450 keV for the 3N-full calculations at saturation density. In comparison, we find a total variation of about 3.6/4.2 MeV when 3NF are completely neglected. Furthermore, Fig. 3 also demonstrates the increased perturbativeness of the many-body expansion. The solid lines show results using the NN ladder sum while the dashed lines use diagrams up to second order. For the NN interaction at N^{2}LO (right panel), diagrams beyond second order in the particle-particle channel give only very small contributions.

The net relative growth of two- and three-body contributions to the energy at two densities are shown in Fig. 4, with and without initial 3NF. The solid lines are

for the N^{3}LO 500 MeV NN potential while the dashed lines are for the N^{2}LO 450/500 MeV potential. The size
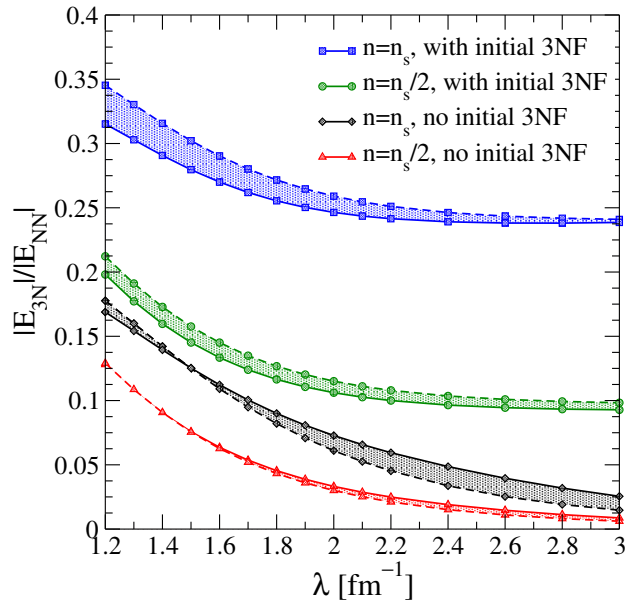
FIG. 4. (Color online) Scaling of the contributions from NN and 3N forces as a function of λ. The dashed lines show the ratio of these two contributions based on the 500 MeV N^{3}LO NN potential [17] and the dashed lines based on the 450/500 MeV N^{2}LO potential [30] (see also Fig. 3).
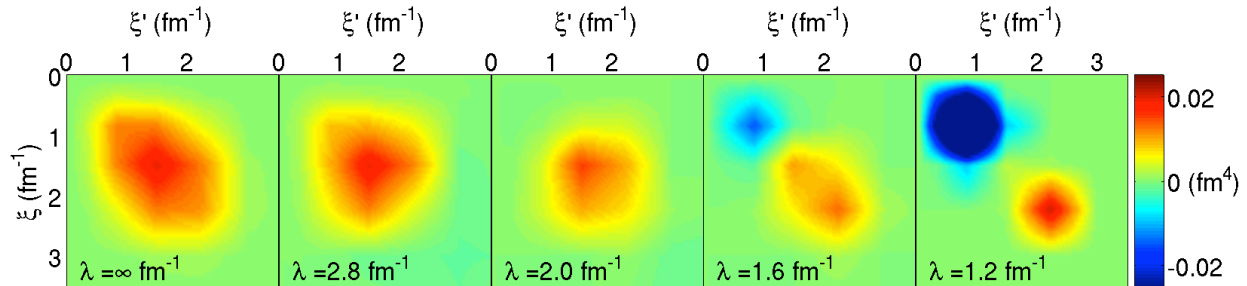
FIG. 5. (Color online) Matrix elements of the evolved 3N potential $\langle \xi \alpha = 1 | \overline{V}_{123} | \xi' \alpha' = 1 \rangle$ (see main text) for $\mathcal{J} = 1/2$, $\mathcal{T} = 3/2$ and positive total parity π_3 at the hyperangle $\theta = \pi/8$. The interactions are the same as in Fig. 1.

of the initial 3NF sets the scale of a natural ratio at that density. It is evident that the change of the net ratio with λ remains natural even down to the smallest values. There is no obvious trend with density; such a trend may be obscured by cancellations among contributions to the net energies.

We can also examine the evolution of the 3NF by looking at slices of the matrix elements. To do this we introduce the hyperradius $\xi^2 = p^2 + 3/4q^2$ and the hyperangle $\tan \theta = 2p/(\sqrt{3}q)$ and visualize the matrix elements as a function of ξ at a fixed hyperangle. A representative example is shown in Fig. 5 for $\theta = \pi/8$ for the dominant partial wave with $\alpha = \alpha'$ and $L = J = S = l = 0$, $T = 1$, $j = 1/2$, $\mathcal{J} = 1/2$ and $\pi_3 = 1$. In this case we observe softening from $\lambda = \infty$ to $\lambda = 2.0$ fm^{-1}. Further evolution causes a strongly attractive part to appear at small momenta; however, its impact will be mitigated by phase space factors. This renormalization merits further study.

In this paper we have presented the first neutron matter calculations based on a fully consistent RG evolution of two- and three-body chiral EFT interactions. Including induced 3NF greatly reduces the resolution scale dependence of the neutron EOS compared to NN-only calculations, with the residual dependence comparable to the expected magnitude of omitted many-body corrections. Thus we are not able to make a definitive statement about the size of induced four-body contributions, but there are no indications of unnatural growth. Future calculations will include both neutron and nuclear matter with higher-order (beyond Hartree-Fock) diagrams including 3NF, which will allow a more complete assessment of higher-body contributions and the range in density for which this framework is reliable. We will also calculate error bands based on uncertainties in the 3NF input. In the future it will be also straightforward to include contributions from 3NF at N^{3}LO [32, 33] once initial matrix elements in partial wave representation are available. This work is currently in progress.

* E-mail: hebeler.4@osu.edu
† E-mail: furnstahl.1@osu.edu

[1] E. Epelbaum, H.-W. Hammer and U.-G. Meissner, Rev. Mod. Phys. **81**, 1773 (2009).
[2] K. Hebeler and A. Schwenk, Phys. Rev. C **82**, 014314 (2010).
[3] I. Tews *et al.*, Phys. Rev. Lett. **110**, 032504 (2013).
[4] T. Krüger *et al.*, in preparation.
[5] K. Hebeler *et al.* Phys. Rev. Lett. **105**, 161102 (2010).
[6] K. Hebeler, Phys. Rev. C **85**, 021002(R) (2012).
[7] E. D. Jurgenson, P. Navratil and R. J. Furnstahl, Phys. Rev. Lett. **103**, 082501 (2009).
[8] E. Anderson *et al.*, Phys. Rev. C **77**, 037001 (2008).
[9] W. Li, E. R. Anderson and R. J. Furnstahl, Phys. Rev. C **84**, 054002 (2011).
[10] E. D. Jurgenson, P. Navratil and R. J. Furnstahl, Phys. Rev. C **83**, 034301, (2011).
[11] S. Binder *et al.*, arXiv:1211.4748 (nucl-th).
[12] G. Hagen *et al.* Phys. Rev. C **76**, 034302 (2007).
[13] K. Tsukiyama, S. K. Bogner, and A. Schwenk, Phys. Rev. C **85**, 061304 (2012).
[14] H. Hergert *et al.*, arXiv:1212.1190 (nucl-th).
[15] V. Soma, C. Barbieri and T. Duguet, Phys. Rev. C **87**, 011303(R) (2013).
[16] T. Otsuka *el al.*, Phys. Rev. Lett. **105**, 032501 (2010).
[17] D. R. Entem and R. Machleidt, Phys. Rev. C **68**, 041001(R) (2003).
[18] R. Roth *et al.*, Phys. Rev. Lett. **109**, 052501 (2012).
[19] R. Roth *et al.*, Phys. Rev. Lett. **107**, 072501 (2011).
[20] S. K. Bogner, R. J. Furnstahl and R. J. Perry, Phys. Rev. C **75**, 061001(R) (2007).
[21] S. K. Bogner, R. J. Furnstahl and A. Schwenk, Prog.

Part. Nucl. Phys. **65**, 94 (2010).

[22] W. Glöckle, *The Quantum Mechanical Few-Body Problem* (Springer-Verlag, Berlin, 1983).

[23] A. Stadler, W. Glöckle and P. U. Sauer, Phys. Rev. C **44**, 2319 (1991).

[24] L. Tolos, B. Friman, A. Schwenk, Nucl. Phys. A **806**, 105 (2008).

[25] J. W. Holt, N. Kaiser and W. Weise, Phys. Rev. C **87**,

014338 (2013).

[26] R. Skibinski *et al.*, Eur. Phys. J **47**, 48 (2011).

[27] J. Golak *et al.*, Eur. Phys. J. A **43**, 241 (2010).

[28] S. K. Bogner *el al.*, Nucl. Phys. A **763**, 59 (2005)

[29] K. Hebeler *et al.*, Phys. Rev. C **83**, 031301(R) (2011).

[30] E. Epelbaum, Prog. Part. Nucl. Phys. **57**, 654 (2006).

[31] N. Kaiser, Eur. Phys. J. A **48**, 135 (2012).

[32] V. Bernard *et al.*, Phys. Rev. C **77**, 064004 (2008).

[33] V. Bernard *et al.*, Phys. Rev. C **84**, 054001 (2011).